

# Valence quark distribution of the pion inside a medium with finite baryon density: A Nambu–Jona-Lasinio model approach

Ashutosh Dwibedi<sup>1, \*</sup> Satyajit Puhan<sup>2, †</sup> Sabyasachi Ghosh<sup>1, ‡</sup> and Harleen Dahiya<sup>2, §</sup>

<sup>1</sup>*Department of Physics, Indian Institute of Technology Bhilai, Kutelabhatta, Durg, 491002, Chhattisgarh, India*

<sup>2</sup>*Department of Physics, Dr. B.R. Ambedkar National Institute of Technology, Jalandhar, 144008, India*

We calculate the in-medium valence quark distribution of the pion immersed in a finite baryon density using the light-cone quark model. The medium-modified pion properties are obtained by using the constituent quark mass-dependent light cone wave functions. To obtain the constituent quark masses at finite baryon density, we employ the two-flavor Nambu–Jona-Lasinio model. We primarily focus on the in-medium electromagnetic form factor, distribution amplitude, and the parton distribution function of the pion. The parton distribution functions are also evolved from the model scale to a perturbative scale using next to leading order Dokshitzer–Gribov–Lipatov–Altarelli–Parisi evolution equations. Furthermore, our calculated form factors are compared with available experimental measurements and lattice quantum chromodynamics studies. We also examine the Mellin moments derived from our parton distribution functions in comparison with existing extractions and theoretical model predictions.

## I. INTRODUCTION

The determination of hadronic properties from the distributions of their constituent partons has long been a central pursuit in nuclear and particle physics [1–7]. Experimental investigations of hadron structure have been primarily carried out through semi-exclusive and inclusive processes [8, 9], while the forthcoming Electron–Ion Collider (EIC) aims to provide unprecedented insight into the partonic structure of hadrons and nuclei [10]. On the theoretical side, numerous studies have explored hadronic properties in vacuum within a variety of effective frameworks [11–28]. While such vacuum studies provide essential benchmarks, understanding the in-medium modification of hadronic properties is equally crucial. This importance arises from at least two considerations. First, medium effects on partonic distributions have been experimentally established. The nuclear structure functions measured in the EMC [29] and SLAC [30] experiments differ from those of free nucleons, highlighting the role of nuclear binding and composition. Likewise, the pion decay constant has been observed to decrease relative to its vacuum value in deeply bound pionic atom measurements [31] and pion–nucleus scattering experiments [32]. Second, in relativistic heavy-ion collisions, hadrons formed at the later stages of the evolution propagate through a medium of finite temperature and baryon density. Their decay and transport properties thus depend on medium-modified parton distributions. In this context, in-medium modifications of bound states have also been investigated from the heavy-ion perspective [33, 34].

The internal structure of hadrons arises from their constituent valence quarks, sea quarks, and gluons, whose distributions are encoded in the distribution amplitudes (DAs), electromagnetic form factors (EMFFs), and parton distribution functions (PDFs). The pion, being the lightest meson and a Goldstone boson of chiral symmetry breaking, has been extensively studied in this context. Numerous investigations have explored its DA [35–38], EMFF [39–42], and PDF [25, 43–46] from both theoretical [25, 35–46] and experimental [47–51] perspectives. The pion DA plays a central role in hard exclusive processes, as it encodes the overlap between the pion state and its valence quark–antiquark Fock component, describing how the pion’s longitudinal momentum is shared between the quark and antiquark. Its normalization yields the pion decay constant, making it a key quantity in hadronic physics. The EMFF, by contrast, characterizes the response of the pion to an electromagnetic probe and provides direct access to its internal charge distribution, including the extraction of the charge radius. The PDF describes the probability of finding a parton carrying a given longitudinal momentum fraction and can be determined from hard inclusive processes such as deep inelastic scattering. The in-medium behavior of these quantities—DA, EMFF, and PDF—has also been studied within various theoretical frameworks [52–62]. In particular, Refs. [52–54] employed the light-cone quark model (LCQM) with constituent quark masses determined from the chiral SU(3) quark mean-field model. Studies in Refs. [55, 56] and [59, 60] utilized the Bethe–Salpeter amplitudes and Gaussian wave functions within the quark–meson coupling (QMC) model, respectively. A hybrid quark–meson coupling and Nambu–Jona-Lasinio (QMC–NJL) model

\* [ashutoshdwibedi92@gmail.com](mailto:ashutoshdwibedi92@gmail.com)

† [puhansatyajit@gmail.com](mailto:puhansatyajit@gmail.com)

‡ [sabya@iitbhilai.ac.in](mailto:sabya@iitbhilai.ac.in)

§ [dahiyah@nitj.ac.in](mailto:dahiyah@nitj.ac.in)

approach was adopted in Refs. [57, 63], whereas Refs. [58, 61] investigated the pion's in-medium structure using the NJL–Bethe–Salpeter equation (NJL–BSE) framework.

In the present work, we investigate the valence parton distribution of the pion following an approach similar to Refs. [52–54], which we call a hybrid light-cone quark model–Nambu–Jona–Lasinio model (LCQM–NJL) framework. In this scheme, the pion properties are described within the LCQM, while the in-medium constituent quark masses are obtained from the two-flavor NJL model. The LCQM effectively incorporates relativistic effects of quarks and gluons inside hadrons and is particularly suitable for studying their properties in the low-momentum, non-perturbative regime of quantum chromodynamics (QCD), where a meson is represented as a superposition of Fock states,

$$|\mathcal{M}\rangle = |q\bar{q}\rangle + |q\bar{q}g\rangle + |q\bar{q}q\bar{q}\rangle + \dots,$$

with the leading component corresponding to the valence quark–antiquark configuration. The LCQM has successfully reproduced the electromagnetic form factor (EMFF) of the pion in agreement with experimental data [64, 65] and has also been used to predict the pion charge radius and decay constant. Given its predictive capability, extending the LCQM to finite-density environments provides a natural means to explore in-medium modifications of pion properties. At finite baryon density or temperature, partial restoration of chiral symmetry occurs, and several effective QCD models—including the chiral quark model, quark–meson model, linear sigma model, and the NJL model—have been employed to study this phenomenon. The NJL model, in particular, has been widely used to describe the properties of quark matter and the quark–gluon plasma (QGP) created in heavy-ion collisions. Its Lagrangian captures quark interactions via four-fermion contact terms and embodies spontaneous chiral symmetry breaking, leading to dynamical mass generation through non-vanishing chiral condensates. The constituent quark masses are determined self-consistently from the gap equation derived from the quark self-energy. The NJL model is most effective in the low-temperature and intermediate-density regimes, where perturbative QCD becomes unreliable due to strong coupling and lattice QCD calculations are hindered by the sign problem. In this work, we employ the two-flavor NJL model to obtain the constituent quark masses at zero temperature and finite baryon density, which are then used to construct the light-front wave functions (LFWFs) for the pion's valence sector. We subsequently investigate the effect of baryon density on the pion's distribution amplitude (DA), decay constant, EMFF, charge radius, parton distribution function (PDF), and Mellin moments, and evolve the in-medium PDFs and Mellin moments from the model scale (0.20 GeV<sup>2</sup>) to the perturbative scale (25 GeV<sup>2</sup>) using the next to leading order Dokshitzer–Gribov–Lipatov–Altarelli–Parisi (NLO DGLAP) evolution equations [66–69].

The present work is organized as follows. In Sec. (II A), we describe the NJL model used in the present work to obtain the in-medium constituent quark masses that have been used as inputs to obtain the properties of pions in the nuclear matter. The LCQM and the LFWFs are briefly addressed in Sec. (II B). In Sec. (III), the results of the present work are discussed and finally summarized in Sec. (IV).

## II. FORMALISM

### A. NJL model and effective quark masses

The Lagrangian of the two-flavor NJL model is given [70–73],

$$\mathcal{L} = \bar{\psi}(i\cancel{\partial} - \mathbf{m})\psi + G [(\bar{\psi}\psi)^2 + (\bar{\psi}i\gamma_5\vec{\sigma}\psi)^2] , \quad (1)$$

where  $\psi \equiv \begin{pmatrix} \psi_u \\ \psi_d \end{pmatrix}$  and  $\mathbf{m} \equiv \begin{pmatrix} m_u \\ m_d \end{pmatrix}$  are the quark fields and bare mass matrix for different flavors, respectively. In this paper, we assume degenerate mass for quark flavors, *i.e.*,  $m_u = m_d = m$ . The Pauli matrices and the coupling constant are respectively denoted by,  $\vec{\sigma}$  and  $G$ . The second term in the square bracket of the NJL Lagrangian (1) captures the quark-quark interaction through effective 4-point contact interactions. The 4-point contact interactions lead to quark self-energy, and one represents the constituent quark mass  $m^*$  *via* the following gap equation,

$$m^* = m + 2iG \int_{\Lambda} \frac{d^4 p}{(2\pi)^4} \text{Tr} S(p) , \quad (2)$$

where  $S(p)$  is the dressed propagator, which is given by  $S(p) = \frac{1}{\cancel{p} - m^* + i\epsilon}$ , the trace in the above equation is taken over color, flavor, and Dirac spaces. The NJL Lagrangian with the contact interaction terms is non-renormalizable, and one introduces a cut-off energy scale  $\Lambda$  to regularize the divergent integrals, which show up in the calculations. For different regularization schemes practiced in the NJL model, readers can refer to [71]. Eq. (2) illustrates the spontaneous breaking of chiral symmetry in which a light current quark mass  $m$  turns into a massive constituent quark mass  $m^*$ . The three model parameters— $m$ ,  $G$ , and  $\Lambda$  are suitably chosen to fit the experimental values of pion mass  $m_{\pi} = 135$  MeV and pion decay constant  $f_{\pi} = 92.4$  MeV in vacuum. We have

chosen the following values for the parameters in the present paper:  $m = 0.0027$  GeV,  $G = 1.95$  GeV $^{-2}$ , and  $\Lambda = 0.95$  GeV. In the presence of a medium at finite chemical potential  $\mu$  and temperature  $T$ , the Gap equation (2) is modified by replacing the vacuum dressed propagator with the in-medium dressed propagator [74],  $S(p, \mu, T) = (\not{p} + m^*) \left[ \frac{1}{p^2 - m^{*2} + i\epsilon} + 2\pi i \delta(p^2 - m^{*2}) (\theta(p_0) f(E_{\mathbf{p}}, \mu) + \theta(-p_0) \bar{f}(E_{\mathbf{p}}, \mu)) \right]$ , where the thermal distribution functions for quarks and anti-quarks are, respectively,  $f(E_{\mathbf{p}}, \mu) = 1/[e^{(E_{\mathbf{p}} - \mu)/T} + 1]$ ,  $\bar{f}(E_{\mathbf{p}}, \mu) = 1/[e^{(E_{\mathbf{p}} + \mu)/T} + 1]$  with  $E_{\mathbf{p}} = \sqrt{\not{p}^2 + m^{*2}}$ . Substituting the in-medium propagator, the gap equation after some simplification reads,

$$m^* = m + 24 G \int_{\Lambda} \frac{d^3 p}{(2\pi)^3} \frac{m^*}{E_{\mathbf{p}}} (1 - f - \bar{f}) . \quad (3)$$

We consider a cold nuclear medium at finite baryon density  $\rho_B$  at zero temperature. In this scenario, the Gap equation (3) can be obtained by replacing the thermal distribution functions  $f \xrightarrow{T=0} \theta(\mu - E_{\mathbf{p}})$ <sup>1</sup>,

$$m^* = m + \frac{6Gm^*}{\pi^2} \left[ \Lambda \sqrt{\Lambda^2 + m^{*2}} - \mu \sqrt{\mu^2 - m^{*2}} - m^{*2} \ln \frac{\Lambda + \sqrt{\Lambda^2 + m^{*2}}}{\mu + \sqrt{\mu^2 - m^{*2}}} \right] . \quad (4)$$

Eq. (4) can be solved to get the constituent quark mass  $m^*$  as a function of quark chemical potential  $\mu$ . One can also readily obtain the constituent quark mass  $m^*$  as a function of baryon density  $\rho_B$  by using  $\mu = \sqrt{\left(\frac{3\pi^2\rho_B}{2}\right)^{2/3} + m^{*2}}$ .

## B. Light-cone quark model

The eigenstate of a meson  $|\mathcal{M}(P^+, \mathbf{P}_{\perp}, S_z)\rangle$  carrying a total four momenta  $P \equiv (P^+, P^-, \mathbf{P}_{\perp})$  and longitudinal spin projection  $S_z$  can be written in the LCQM as follows [11, 75]:

$$|\mathcal{M}(P^+, \mathbf{P}_{\perp}, S_z)\rangle = \sum_{n, \lambda_j} \int \prod_{j=1}^n \frac{dx_j d^2 \mathbf{k}_{\perp j}}{2(2\pi)^3 \sqrt{x_j}} 16\pi^3 \delta\left(1 - \sum_{j=1}^n x_j\right) \delta^{(2)}\left(\sum_{j=1}^n \mathbf{k}_{\perp j}\right) \times \psi_{n/\mathcal{M}}(x_j, \mathbf{k}_{\perp j}, \lambda_j) |n; x_j P^+, x_j \mathbf{P}_{\perp} + \mathbf{k}_{\perp j}, \lambda_j\rangle , \quad (5)$$

where  $x_j = \frac{\mathbf{k}_j^+}{P^+}$ ,  $\mathbf{k}_{\perp j}$  and  $\lambda_j$  are, respectively, the longitudinal momentum fraction, transverse (internal) momentum, and helicity carried by the  $j$ th constituent parton. The delta functions occurring in Eq. (5) ensure the conservation of longitudinal and transverse momentum. The normalization of the multiparticle state  $|n\rangle$  reads as

$$\langle n; k_j'^+, \mathbf{k}_{\perp j}', \lambda_j' | n; k_j^+, \mathbf{k}_{\perp j}, \lambda_j \rangle = \prod_{j=1}^n 16\pi^3 k_j'^+ \delta(k_j'^+ - k_j^+) \delta^{(2)}(\mathbf{k}_{\perp j}' - \mathbf{k}_{\perp j}) \delta_{\lambda_j' \lambda_j} . \quad (6)$$

The  $\psi_{n/\mathcal{M}}(x_j, \mathbf{k}_{\perp j}, \lambda_j)$  are the light-cone wave functions (LCWFs) of the given meson. In general, the eigenstate of a meson can have contributions from the Fock states containing valence quarks as well as sea quarks and gluons. In the following, we consider the two-particle Fock state of the pion consisting only of the valence quarks  $-u$  and  $\bar{d}$ ,

$$|\Pi(P^+, \mathbf{P}_{\perp}, S_z)\rangle = \sum_{\lambda_1, \lambda_2} \int \frac{dx_1 dx_2 d^2 \mathbf{k}_{1\perp} d^2 \mathbf{k}_{2\perp}}{2(2\pi)^3 2(2\pi)^3 \sqrt{x_1 x_2}} 2(2\pi)^3 \delta(1 - x_1 - x_2) \delta^2(\vec{k}_{1\perp} + \vec{k}_{2\perp}) \psi(x_1, x_2, \mathbf{k}_{1\perp}, \mathbf{k}_{2\perp}, \lambda_1, \lambda_2) |x_1 P^+, x_2 P^+, x_1 \vec{P}_{\perp} + \mathbf{k}_{1\perp}, x_2 \vec{P}_{\perp} + \mathbf{k}_{2\perp}, \lambda_1, \lambda_2\rangle ,$$

where we use the kinematic variables with subscripts 1 and 2 for the  $u$ -quark and  $\bar{d}$ -quark, respectively. Simplifying the above integrals by integrating over  $x_2$  and  $\vec{k}_{2\perp}$  we have,

$$|\Pi(P^+, \mathbf{P}_{\perp}, S_z)\rangle = \int \frac{dx d^2 \mathbf{k}_{\perp}}{16\pi^3 \sqrt{x(1-x)}} [\psi(x, \mathbf{k}_{\perp}, \uparrow, \uparrow) |x P^+, \mathbf{k}_{\perp}, \uparrow, \uparrow\rangle + \psi(x, \mathbf{k}_{\perp}, \uparrow, \downarrow) |x P^+, \mathbf{k}_{\perp}, \uparrow, \downarrow\rangle + \psi(x, \mathbf{k}_{\perp}, \downarrow, \uparrow) |x P^+, \mathbf{k}_{\perp}, \downarrow, \uparrow\rangle + \psi(x, \mathbf{k}_{\perp}, \downarrow, \downarrow) |x P^+, \mathbf{k}_{\perp}, \downarrow, \downarrow\rangle] , \quad (7)$$

<sup>1</sup> At zero temperature the thermal part coming from anti-quarks do not contribute at positive baryon density or chemical potential since  $\bar{f} \xrightarrow{T=0} \theta(-\mu - E_{\mathbf{p}})$

where we ignore the subscripts in the momentum labels of the  $u$ -quark. We also suppress the anti-quark labels inside the two-particle Fock basis  $|\rangle$ . Consistent with the constraint  $x_1 + x_2 = 1$ , if the  $u$ -quark carries the  $x$  fraction of the longitudinal momentum, the  $\bar{d}$ -quark will carry  $(1 - x)$  fraction of the total longitudinal momentum. Similarly, the internal part of the transverse momentum of the  $u$  and  $\bar{d}$  are equal in magnitude but opposite in direction. One writes the momenta of the meson and its constituent quarks as,

$$\begin{aligned} P &= \left( P^+, \frac{M^{*2}}{P^+}, \mathbf{0}_\perp \right), \\ k_1 &= \left( xP^+, \frac{\mathbf{k}_\perp^2 + m_u^{*2}}{xP^+}, \mathbf{k}_\perp \right), \\ k_2 &= \left( (1 - x)P^+, \frac{\mathbf{k}_\perp^2 + m_{\bar{d}}^{*2}}{(1 - x)P^+}, -\mathbf{k}_\perp \right), \end{aligned} \quad (8)$$

where  $M^{*2} = \frac{m_u^{*2} + \mathbf{k}_\perp^2}{x} + \frac{m_{\bar{d}}^{*2} + \mathbf{k}_\perp^2}{1-x}$ . Throughout the paper, we take the in-medium quark and anti-quark mass to be the same, i.e.,  $m_u^* = m_{\bar{d}}^* = m^*$ . The LCWFs for pion can be further expressed in terms of momentum space  $\varphi$  and spin  $\mathcal{S}$  wave functions as [76, 77]

$$\psi(x, \mathbf{k}_\perp, \lambda_1, \lambda_2) = \varphi(x, \mathbf{k}_\perp) \mathcal{S}(x, \mathbf{k}_\perp, \lambda_1, \lambda_2), \quad (9)$$

where  $\lambda_1(\lambda_2)$  represent the helicity of the quark (anti-quark). The spin part of the wave function in the light front can be obtained from the instant-form wave function with the aid of Melosh-Wigner rotation [78, 79] or equivalently by choosing the proper quark-meson vertex [80]  $\mathcal{S} = \frac{1}{\sqrt{2M^*}} \bar{u}(xP^+, \mathbf{k}_\perp, \lambda_1) \gamma_5 v((1 - x)P^+, -\mathbf{k}_\perp, \lambda_2)$ ,

$$\begin{aligned} \mathcal{S}(x, \mathbf{k}_\perp, \uparrow, \uparrow) &= -\frac{k_x - ik_y}{\sqrt{2(m^{*2} + \mathbf{k}_\perp^2)}}, \\ \mathcal{S}(x, \mathbf{k}_\perp, \uparrow, \downarrow) &= \frac{m^*}{\sqrt{2(m^{*2} + \mathbf{k}_\perp^2)}}, \\ \mathcal{S}(x, \mathbf{k}_\perp, \downarrow, \uparrow) &= -\frac{m^*}{\sqrt{2(m^{*2} + \mathbf{k}_\perp^2)}}, \\ \mathcal{S}(x, \mathbf{k}_\perp, \downarrow, \downarrow) &= -\frac{k_x + ik_y}{\sqrt{2(m^{*2} + \mathbf{k}_\perp^2)}}. \end{aligned} \quad (10)$$

Adopting the Brodsky-Huang-Lepage prescription [21, 79, 81], the momentum space wave function is given by,

$$\varphi(x, \mathbf{k}_\perp) = A \exp \left[ -\frac{M^{*2} - 2(m_u^{*2} + m_{\bar{d}}^{*2})}{8\beta^2} \right] = A \exp \left[ \frac{m^{*2}}{2\beta^2} \right] \exp \left[ -\frac{m^{*2} + \mathbf{k}_\perp^2}{8x(1-x)\beta^2} \right], \quad (11)$$

where  $A$  and  $\beta$  are the normalization constant and harmonic scale parameter, respectively. One can observe that the spin wave functions in Eq. (10) satisfy the following normalization relation,

$$\sum_{\lambda_1 \lambda_2} \mathcal{S}^*(x, \mathbf{k}_\perp, \lambda_1, \lambda_2) \mathcal{S}(x, \mathbf{k}_\perp, \lambda_1, \lambda_2) = 1. \quad (12)$$

Since the total wavefunction (space and spin) has to be normalized, this gives the following normalization condition for the space part of the wave function,

$$\sum_{\lambda_1 \lambda_2} \int \frac{dxd^2\mathbf{k}_\perp}{2(2\pi)^3} \psi^*(x, \mathbf{k}_\perp, \lambda_1, \lambda_2) \psi(x, \mathbf{k}_\perp, \lambda_1, \lambda_2) = \int \frac{dxd^2\mathbf{k}_\perp}{2(2\pi)^3} |\varphi(x, \mathbf{k}_\perp)|^2 = 1. \quad (13)$$

### III. RESULTS AND DISCUSSION

#### A. In-Medium Constituent Quark Masses

After the discussion on the framework of the NJL model and the LCQM framework to describe the state of the pion in the last two sections, we will now move on to describe its medium-modified DA, PDF, and EMFF. A closer look

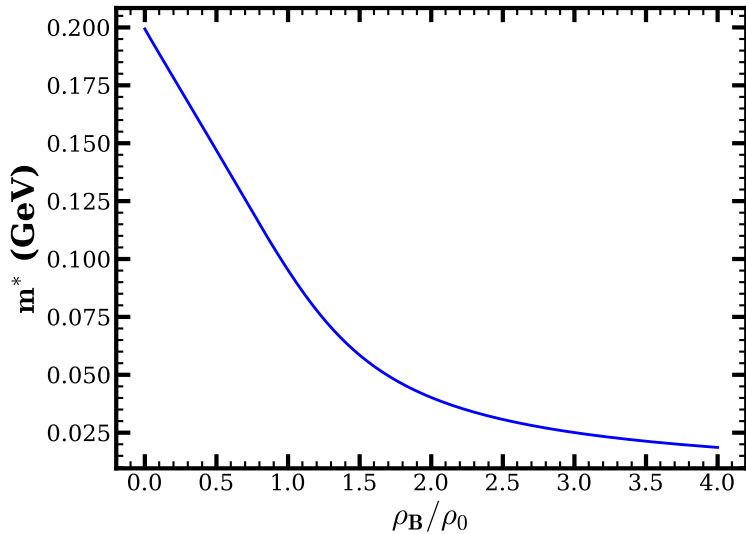


FIG. 1: The constituent quark mass has been plotted as a function of baryonic density  $\rho_B/\rho_0$ .

at the LCWFs reveals that the properties of the pion (up to the valence Fock sector) are fixed by the following two quantities—the mass of the quarks ( $m^*$ ) and the harmonic scale parameter ( $\beta$ ). These quantities are determined from variational methods with the QCD-motivated effective Hamiltonians in vacuum [82]. Once the quark masses are fixed in vacuum ( $\rho_B = 0$ ) from the variational methods, the in-medium ( $\rho_B \neq 0$ ) constituent masses can be obtained from the NJL gap equation. We have assumed the value of the harmonic parameter  $\beta$  to be unchanged in the presence of a medium. In Fig. (1) we show the variation of the constituent quark mass with the baryon density of the medium. The parameters chosen to solve the gap equation are provided in Sec. (II A). We see that the constituent quark mass decreases as the baryon density increases and finally becomes negligible at asymptotically large densities. This behavior is evident as one expects the chiral symmetry to be restored at large baryon densities. Next, we move on to describe the medium-modified DA, PDF, and EMFF for the pion.

### B. Distribution Amplitude (DA)

DA of the pion describes longitudinal momentum sharing between the quark and the anti-quark in its valence Fock state. The information about DAs can be extracted from the hard exclusive processes involving the pion. In terms of the quark field correlators, it is expressed as the vacuum-to-pion matrix element as

$$\langle 0 | \bar{\vartheta}_d(z) i\gamma^+ \gamma^5 \vartheta_u(-z) | \Pi(P^+, \mathbf{P}_\perp) \rangle = i P^+ f_\pi^* \int dx e^{i(x-1/2)P^+ z^-} \phi_{\text{DA}}(x) |_{z^+ = \mathbf{z}_\perp = 0}, \quad (14)$$

where  $\vartheta$ ,  $z = (z^+, z^-, \mathbf{z}_\perp)$ , and  $f_\pi^*$  are the quark field operator, position four vector, and in-medium decay constant. Substitution of the free field operators leads us to the following expression for the correlators,

$$\langle 0 | \bar{\vartheta}_d(z) i\gamma^+ \gamma^5 \vartheta_u(-z) | \Pi(P^+, \mathbf{P}_\perp) \rangle = 2\sqrt{2} i P^+ \int \frac{dx d^2 \mathbf{k}_\perp}{2(2\pi)^3 \sqrt{2x(1-x)}} e^{i(x-1/2)P^+ z^-} (\psi_{\uparrow\downarrow} - \psi_{\downarrow\uparrow}). \quad (15)$$

Introducing the color factor  $\sqrt{N_c}$  in the above equation and equating it with Eq. (14) we have,

$$\frac{f_\pi^*}{2\sqrt{2N_c}} \phi_{\text{DA}}(x) = \int \frac{d^2 \mathbf{k}_\perp}{2(2\pi)^3 \sqrt{2x(1-x)}} (\psi_{\uparrow\downarrow} - \psi_{\downarrow\uparrow}). \quad (16)$$

The DA is normalized as follows,  $\int \phi_{\text{DA}}(x) dx = 1$ , from which one can get the in-medium pion decay constant  $f_\pi^*$ . In Fig. (2)(a) and (b), we display the variation of the DA with respect to the longitudinal momentum fraction  $x$ . In comparison to the vacuum case, we observe that the DA gets flattened (spread out) at non-zero baryon density. Fig. (2)(a) represents the variation of in-medium DA at lower baryon density  $\rho_B = 0 - 1\rho_0$  where as Fig. (2)(b) displays the same but at higher baryon density  $\rho_B = 0 - 4\rho_0$ . At increasing baryon density, we see the universal

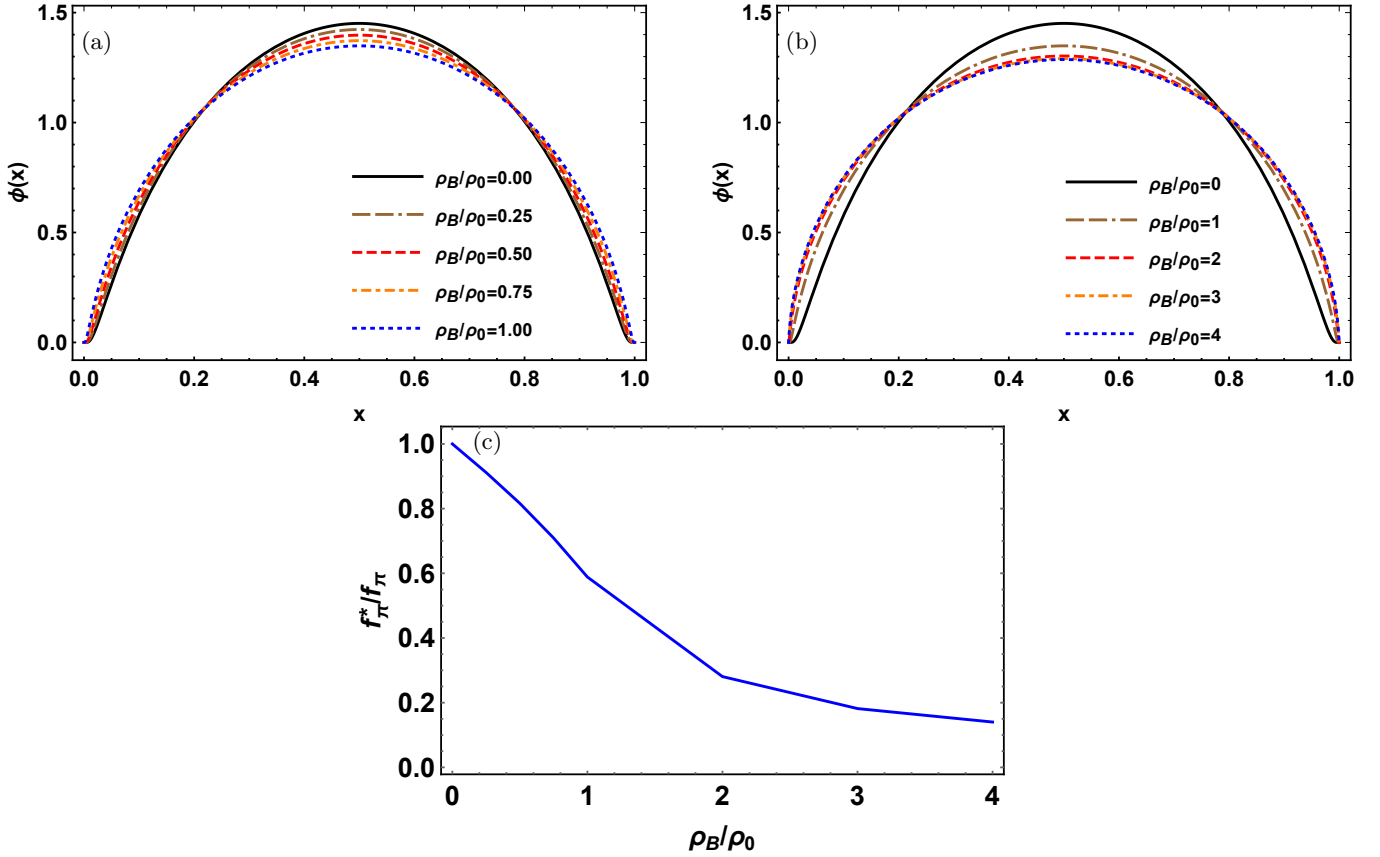


FIG. 2: (Color online) The DA has been plotted with respect to baryonic density up to  $\rho_B/\rho_0 = 1$  in the interval of 0.25 in Fig. (a) and up to baryonic density  $\rho_B/\rho_0 = 4$  in the interval of 1 in Fig. (b). In Fig. (c), we have plotted the ratio of the in-medium decay constant and the vacuum decay constant with respect to the baryonic density  $\rho_B/\rho_0$ . Here all the results are at model scale, i.e, 0.20 GeV<sup>2</sup>.

feature of suppression at mid  $x$  and increment at low and high  $x$  as observed in [54]. Next in Fig. (2)(c), we show the ratio of the in-medium decay constant to the vacuum decay constant of the pion. The results show a monotonic decrease in the decay constant of the pion with increasing baryon density. Even at the nuclear saturation density, we find the in-medium decay constant  $f_\pi^*$  to be approximately 60% of the vacuum value  $f_\pi$ . Similar observations have also been made in Refs. [54, 56, 61]. The expected value of longitudinal momentum, so-called  $\xi$ -moment is defined as

$$\langle \xi^n \rangle = \int_0^1 dx \xi^n \phi_{\text{DA}}(x), \quad (17)$$

with  $\xi = (1 - x) - x = 1 - 2x$ . The inverse moment  $\langle x^{-1} \rangle$  can also be calculated as

$$\langle x^{-1} \rangle = \int_0^1 dx \frac{\phi_{\text{DA}}(x)}{x}. \quad (18)$$

These moments up to  $n = 8$  along with the inverse moment have been presented in Table I. The  $\langle \xi^n \rangle$  moment is found to be increasing with an increase in Baryonic density, and a similar kind of observation is also seen for the case of inverse moment. At free space, the inverse moment is found to be 2.891, which is comparable with the LFHM of 2.62 [14], the Light-front constituent model of 2.82 [83], and the LFQM of 3.11 [84].

### C. Electromagnetic Form Factors (EMFF)

The EMFF gives information about the structure of the bound state system. The physical process that is associated with the EMFF of the pion is  $\pi(P) + \gamma^*(\Delta) \rightarrow \pi(P')$ . The electromagnetic form factors can be obtained from the

$\rho_B/\rho_0$	$\langle \xi^2 \rangle$	$\langle \xi^4 \rangle$	$\langle \xi^6 \rangle$	$\langle \xi^8 \rangle$	$\langle x^{-1} \rangle$
0	0.2029	0.0855	0.0461	0.0282	2.891
1	0.2281	0.1058	0.0619	0.0409	3.233
2	0.2411	0.1171	0.0713	0.0488	3.541
3	0.2445	0.1201	0.0739	0.0510	3.662
4	0.2459	0.1213	0.0749	0.0519	3.720

TABLE I: The  $\langle \xi^n \rangle$  moment up to  $n = 8$  and inverse moment have been predicted at different baryonic densities up to  $\rho_B/\rho_0 = 4$  at the model scale.

GPD  $H$  by integrating over the longitudinal momentum fraction at zero skewness. For the pion, the chirally even GPD is given by,

$$H(x, \xi, t) = \frac{1}{2} \int \frac{dz^-}{4\pi} e^{ixP^+z^-/2} \langle \Pi(P', \lambda') | \bar{\vartheta}_u(0) \gamma^+ \vartheta_u(z) | \Pi(P, \lambda) \rangle |_{z^+ = \mathbf{z}_\perp = 0}, \quad (19)$$

where momentum transfer  $\Delta = P' - P$  ( $t \equiv \Delta^2 \equiv -Q^2$ ) and skewness  $\xi = -\frac{\Delta^+}{2P^+}$ . We evaluate the form factor in terms of the GPD at  $\xi = 0$  as,

$$\begin{aligned} F(Q^2) &= e_u F^u(Q^2) + e_{\bar{d}} F^{\bar{d}}(Q^2) \\ &= e_u \int H(x, 0, t) dx + e_{\bar{d}} \int H(1-x, 0, t) dx. \end{aligned} \quad (20)$$

Fig. (3)(a) represents the variation of the EMFFs  $F(Q^2)$  at different baryon densities upto  $\rho_B/\rho_0 = 1$ . The variation of the scaled EMFFs  $Q^2 F(Q^2)$  for the same values of baryon densities has also been shown in Fig. (3)(b). This essentially magnifies the difference between different baryon density curves for  $Q^2 > 1 \text{ GeV}^2$ . Next in Fig. (3)(c), we compare our results with the available vacuum experimental data [49, 85–88] and with lattice calculations [89, 90] in Fig. (3)(d) and (e). The same is shown in Fig. (4), albeit with larger values of baryon density (up to  $4\rho_0$ ). We see a consistent suppression of in-medium EMFFs (across the momentum scale  $Q^2 \approx 0 - 10 \text{ GeV}^2$ ) as compared to vacuum EMFF derived within our hybrid LCQM-NJL approach. To end the discussion on the EMFFs, we show the important quantity charge radii in Fig. (4)(f), which is defined with the help of EMFF as

$$\begin{aligned} \langle r_\pi^2 \rangle &= e_u \langle r_u^2 \rangle + e_{\bar{d}} \langle r_{\bar{d}}^2 \rangle \\ &= -e_u 6 \frac{\partial F^u(Q^2)}{\partial Q^2} |_{Q^2 \rightarrow 0} - e_{\bar{d}} 6 \frac{\partial F^{\bar{d}}(Q^2)}{\partial Q^2} |_{Q^2 \rightarrow 0}. \end{aligned} \quad (21)$$

We observe that the charge radii increase rapidly with increasing baryon density and slowly saturate around 0.5 fm as  $\rho_B > 3\rho_0$ .

#### D. Parton Distribution Function (PDF)

The PDF of the pion is the probability of finding the quark at a certain longitudinal momentum. It appears in the scattering cross-section of deep inclusive processes. The leading twist PDF for the pion can be obtained from the transverse momentum integrated leading twist TMD. The leading twist TMD for the quark in the pion is defined by,

$$\Phi(x, \mathbf{k}_\perp) = \frac{1}{2} \int \frac{dz^- d^2 \mathbf{z}^\perp}{2(2\pi)^3} e^{ik \cdot z} \langle \Pi(P, \lambda) | \bar{\vartheta}_u(0) \gamma^+ \vartheta_u(z) | \Pi(P, \lambda) \rangle. \quad (22)$$

The unpolarized PDF obtained from the above TMD is given by,

$$\begin{aligned} f_1(x) &= \int d^2 \mathbf{k}_\perp \Phi(x, \mathbf{k}_\perp) \\ &= \int \frac{d^2 \mathbf{k}_\perp}{16\pi^3} (|\psi(x, \mathbf{k}_\perp, \uparrow, \uparrow)|^2 + |\psi(x, \mathbf{k}_\perp, \uparrow, \downarrow)|^2 + |\psi(x, \mathbf{k}_\perp, \downarrow, \downarrow)|^2 + |\psi(x, \mathbf{k}_\perp, \downarrow, \uparrow)|^2). \end{aligned} \quad (23)$$

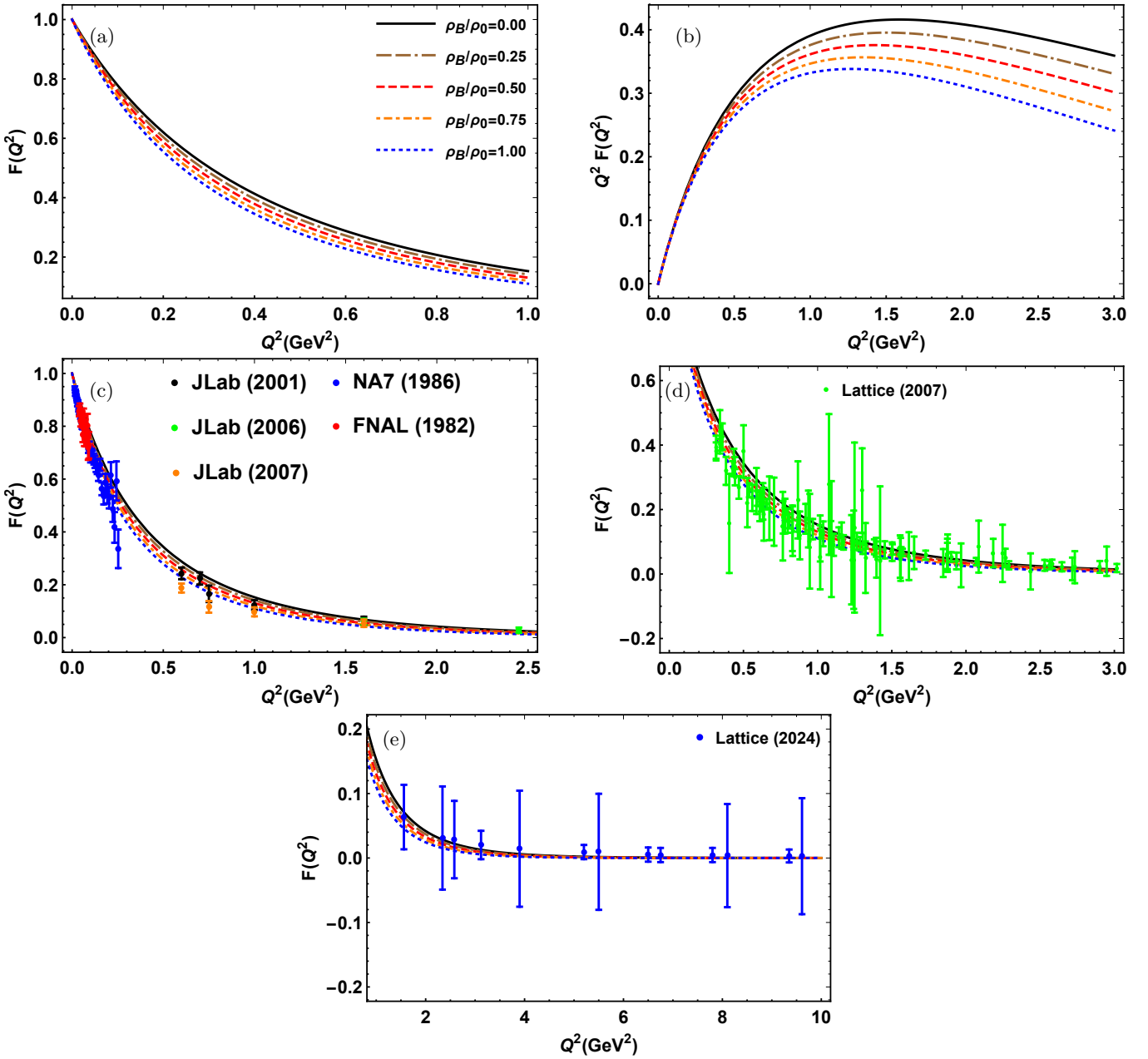


FIG. 3: (Color online) The electro-magnetic form factor of pion has been plotted with respect to  $Q^2$  GeV $^2$  at different baryonic densities up to  $\rho_B/\rho_0 = 1$  in Fig. (a) and (b). Both the in-medium and vacuum FFs have been compared with available vacuum experimental data [49, 85–88] in Fig. (c) along with lattice simulations [89, 90] in Fig. (d) and (e).

In Fig. (5)(a), we show the variation of the scaled PDF  $xf_1(x)$  for quarks with respect to longitudinal momentum fraction  $x$  at different baryon densities at the model scale. Fig. (5)(b) contains the same information at higher baryon densities  $\rho_B \leq 4\rho_0$ . We also provide the PDF at zero baryon density (black curve) for the sake of comparison. From the quark PDF  $f_1$  we can calculate the anti quark PDF  $\bar{f}_1$  by replacing  $x$  by  $1 - x$ , i.e.,  $\bar{f}_1(x) = f(1 - x)$ . The PDFs at model scale obey the sum rule  $\int f_1(x) dx = 1$  and  $\int \bar{f}_1(1 - x) dx = 1$ . One observes that with increasing baryon density, the peak of the quark PDF shifts to the right, i.e., to higher values of  $x$ . This suggests an increase in the probability of finding the  $u$ -quark at higher longitudinal momentum inside a baryon-rich medium compared to the vacuum. Till now, the results of the PDF are shown at a model scale of 0.20 GeV $^2$ . To see the longitudinal momentum fractions carried by quarks at a higher momentum scale, we evolved the  $u$ -quark PDF from model scale to a scale of 25 GeV $^2$  using NLO DGLAP equations. The variation of evolved  $u$ -quark PDF has been shown in Fig. (5)(c). See

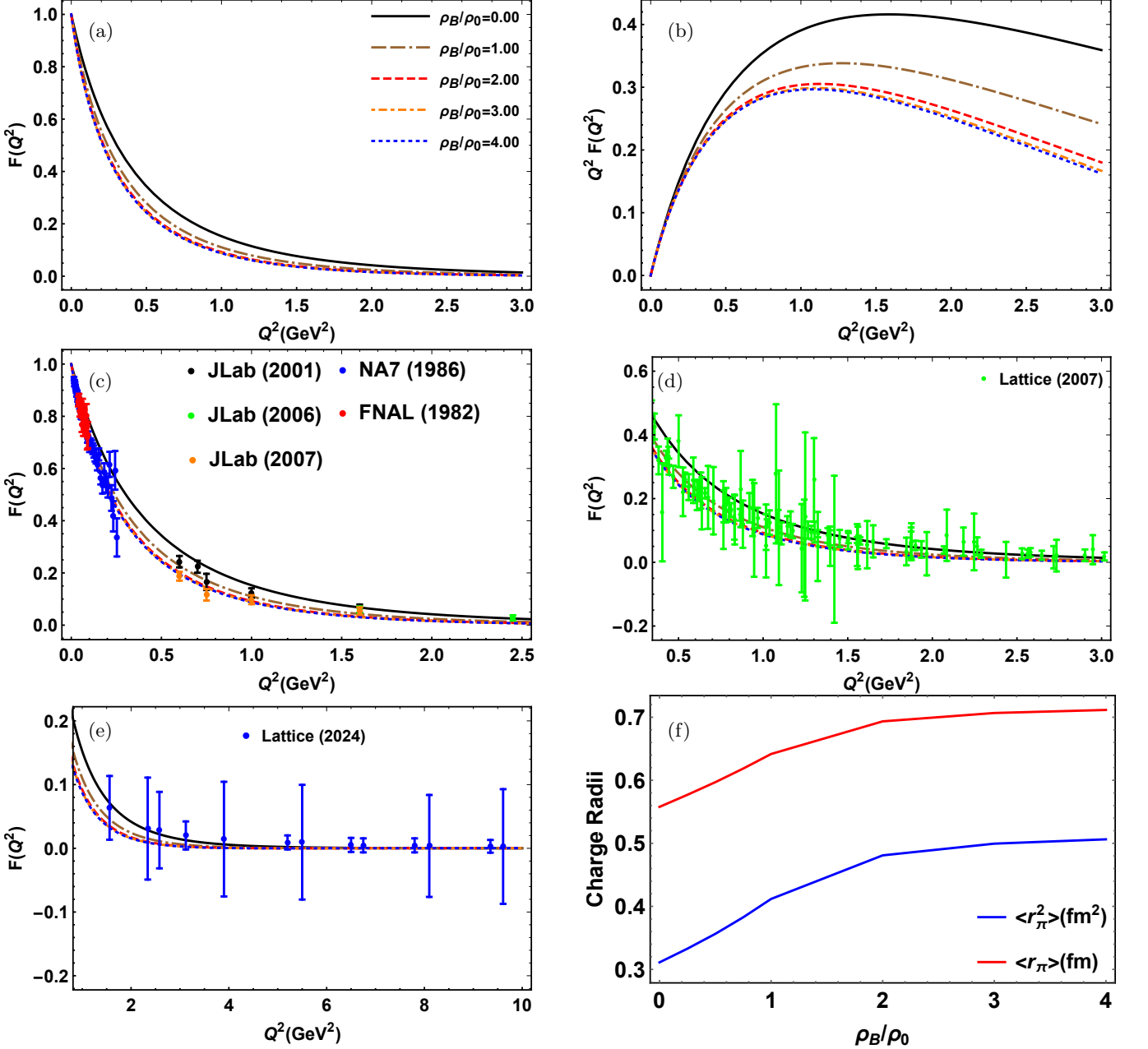


FIG. 4: (Color online) The pion FFs have been plotted with respect to  $Q^2$  GeV $^2$  at different baryonic densities up to  $\rho_B/\rho_0 = 4$  in Fig. (a) and (b). Both the in-medium and vacuum FFs have been compared with available vacuum experimental data [49, 85–88] in Fig. (c) along with lattice simulations [89, 90] in Fig. (d) and (e). Fig. (f) shows the variation of the in-medium pion charge radius along with the squared charge radius with respect to the baryonic density  $\rho_B/\rho_0$ .

that the magnitude of the evolved PDF is smaller for most values of  $x$  (except at lower  $x$ ) compared to the PDF evaluated at the model scale. In contrast to the PDF observed in the model scale, here we see a very slight shift of the peak toward higher longitudinal momentum at increasing baryon density. Also, a very small variation among the PDFs at different baryon densities and vacuum is observed. From this behavior, one can conclude that the effect of dense medium on the PDF is less at high momentum scale (perturbative regime) than at the non-perturbative model scale. Subsequently, we display the in-medium Mellin moments  $\langle x^n \rangle$  of quark PDFs, which encode non-perturbative aspects of QCD. The first moment ( $n = 1$ ) corresponds to the average momentum fraction carried by the quark inside the pion. The higher-order Mellin moments give information about the quark densities with respect to different

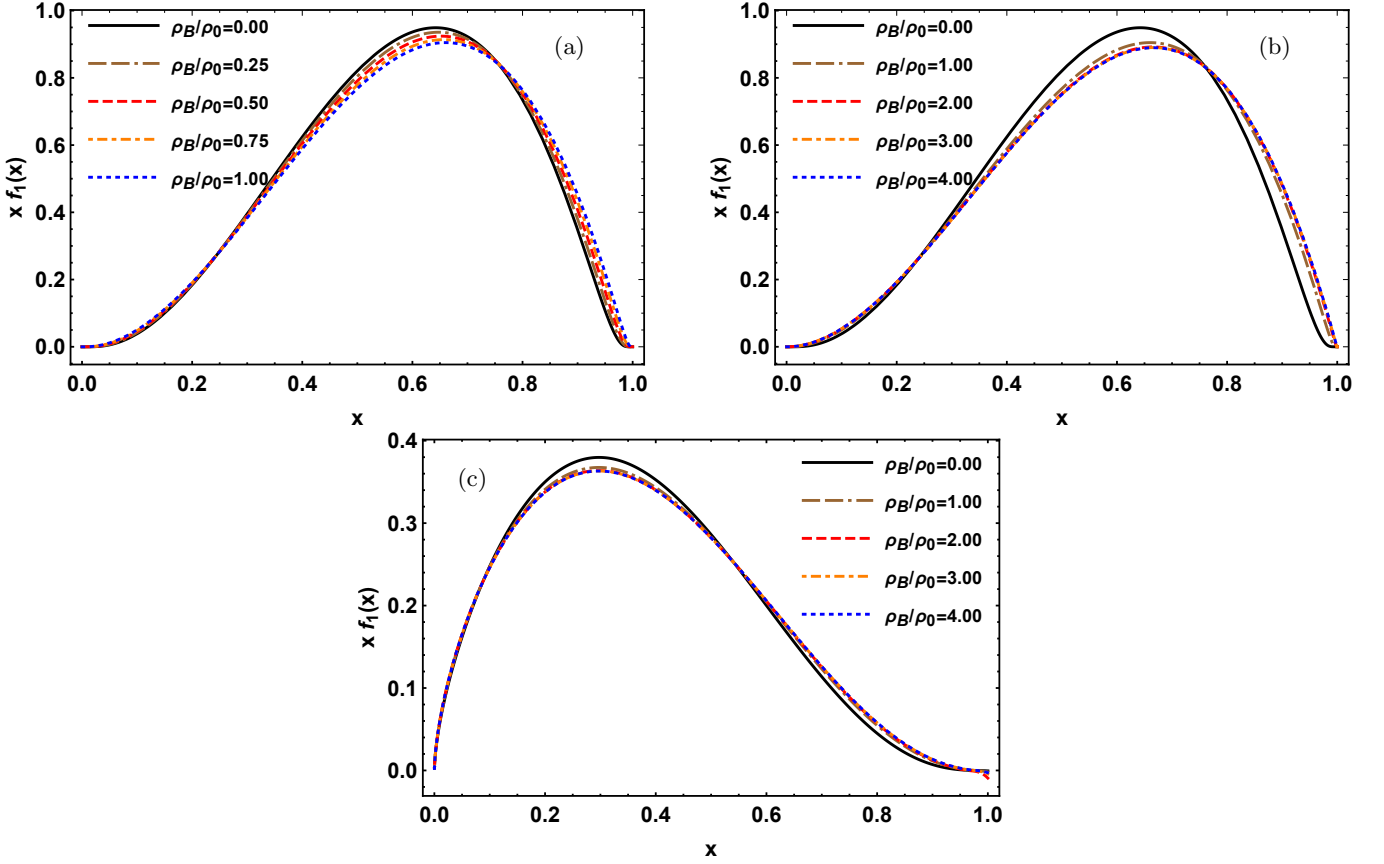


FIG. 5: (Color online) The unpolarized pion PDFs  $f_1(x)$  have been plotted at different baryonic densities with respect to  $x$  in Fig. (a) and (b) at the model scale. In Fig. (c), we have plotted the in-medium evolved PDFs at  $25 \text{ GeV}^2$  using the NLO DGLAP equation.

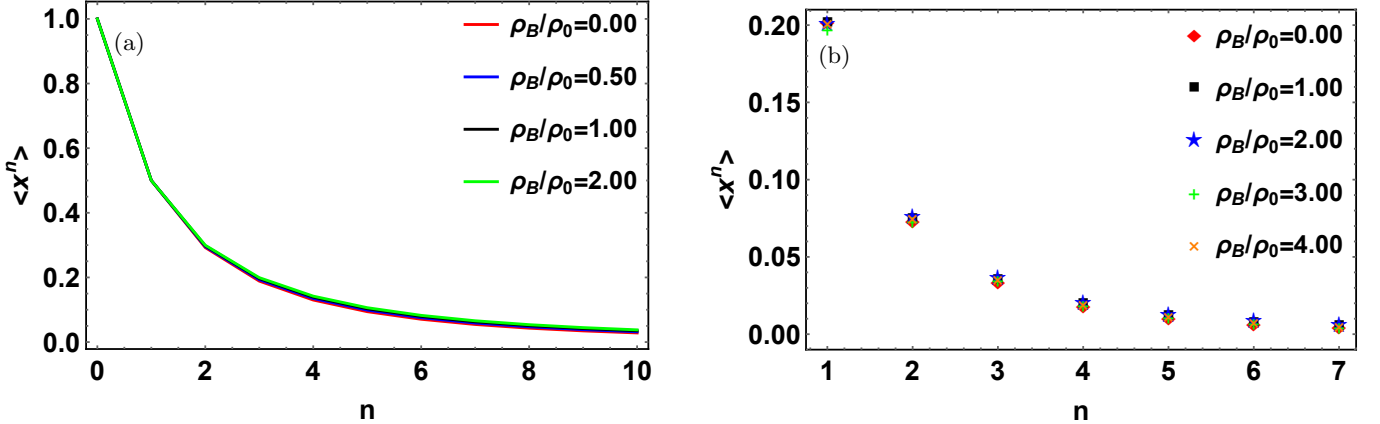


FIG. 6: (Color online) The in-medium Mellin moment  $\langle x^n \rangle$  at different baryonic densities has been calculated up to  $n = 10$  at the model scale in Fig. (a) and at  $25 \text{ GeV}^2$  in Fig. (b).

momentum fractions. The Mellin moments  $\langle x^n \rangle$  are calculated as [91],

$$\langle x^n \rangle = \int x^n f_1(x) dx . \quad (24)$$

We see marginal changes in the Mellin moments with a change in baryon densities both in the model scale (Fig. (6)(a)) and evolved scale (Fig. (6)(b)). Also comparing with lattice QCD predictions of the pion Mellin moment at  $Q^2 = 2$

$2\langle x \rangle$	$Q^2$ (GeV $^2$ )					
	1.69	4	5	5.76	27	49
This work	0.50	0.46	0.44	0.44	0.40	0.38
JAM global fit [93]	$0.54 \pm 0.01$	-	$0.48 \pm 0.01$	-	-	-
JAM DY [93]	$0.60 \pm 0.01$					
xFitter [94]	$0.55 \pm 0.06$	$0.50 \pm 0.05$	$0.49 \pm 0.05$	$0.48 \pm 0.05$	$0.42 \pm 0.04$	$0.41 \pm 0.04$
Lattice-1 [95]	-	$0.428 \pm 0.03$	-	-	-	-
SMRS [99]	-	0.47	-	-	-	$0.49 \pm 0.02$
Han [100]	-	$0.51 \pm 0.03$	-	-	-	-
GRVPI1 [101]	-	0.39	-	-	-	-
Ding [102]	-	$0.48 \pm 0.03$	-	-	-	-
Lattice-2 [96]	-	-	-	$0.558 \pm 0.166$	-	-
Lattice-3 [97]	-	-	-	$0.48 \pm 0.04$	-	-
WRH [50]	-	-	-	-	$0.434 \pm 0.022$	-
ChQM-1 [103]	-	-	-	-	0.428	
ChQM-2 [104]	-	-	-	-	0.46	-
Lattice-4 [98]	-	-	-	-	-	$0.46 \pm 0.05$
BLFQ-NJL [25]	$0.54 \pm 0.02$	$0.49 \pm 0.018$	-	$0.47 \pm 0.018$	$0.42 \pm 0.016$	$0.40 \pm 0.015$

TABLE II: We have compared our total average longitudinal momentum fraction  $2\langle x \rangle$  carried by the valence quark antiquark at  $Q^2 = 1.69, 4, 5, 5.76, 27$  and  $49$  GeV $^2$  through NLO DGLAP evolution with JAM extraction [93], xFitter [94], Lattice data [95–98] and theoretical models [25, 50, 99–104].

GeV $^2$ , we found that  $\langle x \rangle = 0.243$  and  $\langle x^2 \rangle = 0.098$  compared to  $\langle x \rangle = 0.261$  and  $\langle x^2 \rangle = 0.082$ , respectively [92]. We have also predicted the total valence quark contribution  $2\langle x \rangle$  to the total momentum fraction of the pion in Table II at different energy scales in vacuum. We found that at  $Q^2 = 49$  GeV $^2$ , only 38% of the momentum fraction carried by the quark antiquark, the remaining 62% will be carried by the gluon and sea-quarks. At different energy scales, we have compared our results with JAM extraction [93], xFitter [94], Lattice data [95–98], and theoretical models [25, 50, 99–104].

#### IV. SUMMARY

To summarize the work, we have studied the in-medium properties of the pion by determining the quark distribution amplitude, electromagnetic form factor, and parton distribution function. To encode the dense-medium effects on the pion, we use the Nambu–Jona-Lasinio model and obtain the constituent quark masses as a function of baryon density. Whereas the quark-antiquark bound state has been described by the light-cone quark model. We restrict ourselves to the valence Fock sector and express the light cone wave functions that implicitly depend on the baryon density of the surrounding medium via the constituent quark mass. We observe that the constituent quark mass decreases with an increase in baryon density as a result of partial restoration of chiral symmetry. Subsequently, we have solved the quark field correlators to get the distribution amplitude, electromagnetic form factor, and parton distribution function in terms of the light cone wave functions. In the presence of a dense medium, the distribution amplitude is observed to be suppressed for the intermediate longitudinal momentum fraction ( $\sim 0.2\text{--}0.8$ ) and enhanced at low or high longitudinal momentum fraction. The decay constant is observed to be less than the vacuum decay constant, consistent with the earlier predictions. The electromagnetic form factor in vacuum is observed to decrease with the momentum transfer, in par with several experimental and lattice studies. The in-medium form factor is suppressed from the corresponding vacuum values for the intermediate range of momentum transfer (0.1–1.5 GeV $^2$ ) and merges with the vacuum results for very low or high momentum transfer. In the limit of vanishing momentum transfer, the variation in the form factor is encoded in the charge radii of the pion. For relatively lower values of baryon densities ( $\rho_B/\rho_0 \sim 0\text{--}2$ ), we observe a rapid increase in the charge radii as a function of baryon density, and it slowly saturates at high baryon density. We have also analyzed the unpolarized parton distribution functions for pions in vacuum and in a medium with finite baryon density, both at model scale and evolved scale of 25 GeV $^2$ . To get the evolved parton distribution function, the next to leading order Dokshitzer–Gribov–Lipatov–Altarelli–Parisi equations are used. In a vacuum, the parton distribution function increases with the increase in longitudinal momentum fraction, has a peak (approximately around 0.65), and then decreases. It is observed that in a dense medium, for intermediate values of the

longitudinal momentum fractions (approximately, 0.4-0.75), the parton distribution function is suppressed, whereas for other values it is enhanced. The peak of the parton distribution function is also observed to shift towards higher longitudinal momentum fractions with an increase in the density of the surrounding medium. Although some similar medium effects persist in the evolved parton distribution functions, it is marginal compared to the model scale. The effect of the baryon density of the medium on the Mellin moments is seen to be minimal both in the model and perturbative scale.

## V. ACKNOWLEDGEMENT

This work was partially supported by the Ministry of Education (MoE), Govt. of India (A.D., S.P.); Board of Research in Nuclear Sciences (BRNS) and Department of Atomic Energy (DAE), Govt. of India, under Grant No. 57/14/01/2024-BRNS/313 (S.G.); and the Science and Engineering Research Board, Anusandhan-National Research Foundation, Government of India, under the scheme SERB-POWER Fellowship (Ref No. SPF/2023/000116) (H.D.).

---

[1] J. Polchinski and M. J. Strassler, Deep inelastic scattering and gauge / string duality, *JHEP* **05**, 012, arXiv:hep-th/0209211.

[2] G. Altarelli and G. Parisi, Asymptotic Freedom in Parton Language, *Nucl. Phys. B* **126**, 298 (1977).

[3] H.-L. Lai, M. Guzzi, J. Huston, Z. Li, P. M. Nadolsky, J. Pumplin, and C. P. Yuan, New parton distributions for collider physics, *Phys. Rev. D* **82**, 074024 (2010), arXiv:1007.2241 [hep-ph].

[4] M. Diehl, Introduction to GPDs and TMDs, *Eur. Phys. J. A* **52**, 149 (2016), arXiv:1512.01328 [hep-ph].

[5] A. V. Belitsky and A. V. Radyushkin, Unraveling hadron structure with generalized parton distributions, *Phys. Rept.* **418**, 1 (2005), arXiv:hep-ph/0504030.

[6] M. Garcon, An Introduction to the generalized parton distributions, *Eur. Phys. J. A* **18**, 389 (2003), arXiv:hep-ph/0210068.

[7] M. Diehl, Generalized parton distributions, *Phys. Rept.* **388**, 41 (2003), arXiv:hep-ph/0307382.

[8] M. K. Jones *et al.* (Jefferson Lab Hall A),  $G_{Ep}/G_{Mp}$  ratio by polarization transfer in  $\vec{e}p \rightarrow e\vec{p}$ , *Phys. Rev. Lett.* **84**, 1398 (2000), arXiv:nucl-ex/9910005.

[9] S. Amoroso *et al.*, Snowmass 2021 Whitepaper: Proton Structure at the Precision Frontier, *Acta Phys. Polon. B* **53**, 12 (2022), arXiv:2203.13923 [hep-ph].

[10] R. Abdul Khalek *et al.*, Science Requirements and Detector Concepts for the Electron-Ion Collider: EIC Yellow Report, *Nucl. Phys. A* **1026**, 122447 (2022), arXiv:2103.05419 [physics.ins-det].

[11] S. J. Brodsky, G. F. de Teramond, H. G. Dosch, and J. Erlich, Light-Front Holographic QCD and Emerging Confinement, *Phys. Rept.* **584**, 1 (2015), arXiv:1407.8131 [hep-ph].

[12] G. F. de Teramond and S. J. Brodsky, Light-Front Holography: A First Approximation to QCD, *Phys. Rev. Lett.* **102**, 081601 (2009), arXiv:0809.4899 [hep-ph].

[13] S. Puhan and H. Dahiya, Leading twist T-even TMDs for the spin-1 heavy vector mesons, *Phys. Rev. D* **109**, 034005 (2024), arXiv:2310.03465 [hep-ph].

[14] S. Puhan, S. Sharma, N. Kaur, N. Kumar, and H. Dahiya, T-even TMDs for the spin-0 pseudo-scalar mesons upto twist-4 using light-front formalism, *JHEP* **02**, 075, arXiv:2310.03464 [hep-ph].

[15] R. Acharyya, S. Puhan, and H. Dahiya, Quark spin-orbit correlations in spin-0 and spin-1 mesons using the light-front quark model, *Phys. Rev. D* **110**, 034020 (2024), arXiv:2405.00446 [hep-ph].

[16] S. Sharma, S. Puhan, N. Kumar, and H. Dahiya, TMD Relations: Insights from a Light-Front Quark-Diquark Model, *PTEP* **2024**, 103B05 (2024), arXiv:2405.13727 [hep-ph].

[17] R. Acharyya, S. Puhan, H. Dahiya, and N. Kumar, Spectroscopy of excited quarkonium states in the light-front quark model\*, *Chin. Phys. C* **49**, 023104 (2025), arXiv:2408.07715 [hep-ph].

[18] S. Puhan, N. Kaur, and H. Dahiya, Transverse and spatial structure of light to heavy pseudoscalar mesons in light-cone quark model, *Phys. Rev. D* **111**, 014008 (2025), arXiv:2410.07596 [hep-ph].

[19] S. Puhan and H. Dahiya, Scalar, vector, and tensor form factors of pion and kaon, *Phys. Rev. D* **111**, 114039 (2025), arXiv:2505.02507 [hep-ph].

[20] S. Kaur, C. Mondal, and H. Dahiya, Light-front holographic  $\rho$ -meson distributions in the momentum space, *JHEP* **01**, 136, arXiv:2009.04288 [hep-ph].

[21] S. Kaur, N. Kumar, J. Lan, C. Mondal, and H. Dahiya, Tomography of light mesons in the light-cone quark model, *Phys. Rev. D* **102**, 014021 (2020), arXiv:2002.01199 [hep-ph].

[22] S. Kaur and H. Dahiya, Study of kaon structure using the light-cone quark model, *Phys. Rev. D* **100**, 074008 (2019), arXiv:1908.01939 [hep-ph].

[23] S. Kaur and H. Dahiya, Wigner distributions and GTMDs in a proton using light-front quark-diquark model, *Nucl. Phys. B* **937**, 272 (2018), arXiv:1810.09099 [hep-ph].

[24] J. Lan, C. Mondal, S. Jia, X. Zhao, and J. P. Vary, Parton Distribution Functions from a Light Front Hamiltonian and QCD Evolution for Light Mesons, *Phys. Rev. Lett.* **122**, 172001 (2019), arXiv:1901.11430 [nucl-th].

[25] J. Lan, C. Mondal, S. Jia, X. Zhao, and J. P. Vary, Pion and kaon parton distribution functions from basis light front quantization and QCD evolution, *Phys. Rev. D* **101**, 034024 (2020), arXiv:1907.01509 [nucl-th].

[26] D. Chakrabarti and C. Mondal, Generalized Parton Distributions for the Proton in AdS/QCD, *Phys. Rev. D* **88**, 073006 (2013), arXiv:1307.5128 [hep-ph].

[27] J. More, A. Mukherjee, S. Nair, and S. Saha, Gluon contribution to the mechanical properties of a dressed quark in light-front Hamiltonian QCD, *Phys. Rev. D* **107**, 116005 (2023), arXiv:2302.11906 [hep-ph].

[28] W. Qian and B.-Q. Ma, Vector meson omega-phi mixing and their form factors in light-cone quark model, *Phys. Rev. D* **78**, 074002 (2008), arXiv:0809.4411 [hep-ph].

[29] J. J. Aubert *et al.* (European Muon), The ratio of the nucleon structure functions  $F_2^N$  for iron and deuterium, *Phys. Lett. B* **123**, 275 (1983).

[30] R. G. Arnold *et al.*, Measurements of the A-Dependence of Deep Inelastic electron Scattering from Nuclei, *Phys. Rev. Lett.* **52**, 727 (1984).

[31] K. Suzuki *et al.*, Precision spectroscopy of pionic 1s states of Sn nuclei and evidence for partial restoration of chiral symmetry in the nuclear medium, *Phys. Rev. Lett.* **92**, 072302 (2004), arXiv:nucl-ex/0211023.

[32] E. Friedman *et al.*, The In-medium isovector  $\pi N$  amplitude from low energy pion scattering, *Phys. Rev. Lett.* **93**, 122302 (2004), arXiv:nucl-ex/0404031.

[33] R. Sharma, I. Vitev, and B.-W. Zhang, Light-cone wave function approach to open heavy flavor dynamics in QCD matter, *Phys. Rev. C* **80**, 054902 (2009), arXiv:0904.0032 [hep-ph].

[34] J. Zhao *et al.*, Hadronization of heavy quarks, *Phys. Rev. C* **109**, 054912 (2024), arXiv:2311.10621 [hep-ph].

[35] A. V. Radyushkin, Shape of Pion Distribution Amplitude, *Phys. Rev. D* **80**, 094009 (2009), arXiv:0906.0323 [hep-ph].

[36] M. V. Polyakov, On the Pion Distribution Amplitude Shape, *JETP Lett.* **90**, 228 (2009), arXiv:0906.0538 [hep-ph].

[37] J.-H. Zhang, J.-W. Chen, X. Ji, L. Jin, and H.-W. Lin, Pion Distribution Amplitude from Lattice QCD, *Phys. Rev. D* **95**, 094514 (2017), arXiv:1702.00008 [hep-lat].

[38] S.-S. Xu, L. Chang, C. D. Roberts, and H.-S. Zong, Pion and kaon valence-quark parton quasidistributions, *Phys. Rev. D* **97**, 094014 (2018), arXiv:1802.09552 [nucl-th].

[39] C. D. Roberts, Electromagnetic pion form-factor and neutral pion decay width, *Nucl. Phys. A* **605**, 475 (1996), arXiv:hep-ph/9408233.

[40] B. Ananthanarayan, I. Caprini, and D. Das, Pion electromagnetic form factor at high precision with implications to  $a_\mu^{\pi\pi}$  and the onset of perturbative QCD, *Phys. Rev. D* **98**, 114015 (2018), arXiv:1810.09265 [hep-ph].

[41] E. Ydrefors, W. de Paula, J. H. A. Nogueira, T. Frederico, and G. Salmé, Pion electromagnetic form factor with Minkowskian dynamics, *Phys. Lett. B* **820**, 136494 (2021), arXiv:2106.10018 [hep-ph].

[42] L. Chang, I. C. Cloét, C. D. Roberts, S. M. Schmidt, and P. C. Tandy, Pion electromagnetic form factor at spacelike momenta, *Phys. Rev. Lett.* **111**, 141802 (2013), arXiv:1307.0026 [nucl-th].

[43] L. Chang and A. W. Thomas, Pion valence-quark parton distribution function, *Physics Letters B* **749**, 547 (2015).

[44] J.-H. Zhang, J.-W. Chen, L. Jin, H.-W. Lin, A. Schäfer, and Y. Zhao, First direct lattice-QCD calculation of the  $x$ -dependence of the pion parton distribution function, *Phys. Rev. D* **100**, 034505 (2019), arXiv:1804.01483 [hep-lat].

[45] C. Shi, C. Mezrag, and H.-s. Zong, Pion and kaon valence quark distribution functions from Dyson-Schwinger equations, *Phys. Rev. D* **98**, 054029 (2018), arXiv:1806.10232 [nucl-th].

[46] C. Chen, L. Chang, C. D. Roberts, S. Wan, and H.-S. Zong, Valence-quark distribution functions in the kaon and pion, *Phys. Rev. D* **93**, 074021 (2016), arXiv:1602.01502 [nucl-th].

[47] S. A. et al., A measurement of the space-like pion electromagnetic form factor, *Nuclear Physics B* **277**, 168 (1986).

[48] L. Barkov, A. Chilingarov, S. Eidelman, B. Khazin, M. Lelchuk, V. Okhapkin, E. Pakhtusova, S. Redin, N. Ryskulov, Y. Shatunov, A. Shekhtman, B. Shwartz, V. Sidorov, A. Skrinsky, V. Smakhtin, and E. Solodov, Electromagnetic pion form factor in the timelike region, *Nuclear Physics B* **256**, 365 (1985).

[49] J. Volmer *et al.* (Jefferson Lab  $F_\pi$ ), Measurement of the Charged Pion Electromagnetic Form-Factor, *Phys. Rev. Lett.* **86**, 1713 (2001), arXiv:nucl-ex/0010009.

[50] K. Wijesooriya, P. E. Reimer, and R. J. Holt, The pion parton distribution function in the valence region, *Phys. Rev. C* **72**, 065203 (2005), arXiv:nucl-ex/0509012.

[51] B. Aubert *et al.* (BaBar), Measurement of the  $\gamma\gamma^* \rightarrow \pi^0$  transition form factor, *Phys. Rev. D* **80**, 052002 (2009), arXiv:0905.4778 [hep-ex].

[52] S. Puhan, N. Kaur, A. Kumar, S. Dutt, and H. Dahiya, Effect of nuclear medium on the spatial distribution of pions, *Nucl. Phys. B* **1017**, 116940 (2025), arXiv:2501.16706 [hep-ph].

[53] N. Kaur, S. Puhan, R. Pandey, A. Kumar, S. Dutt, and H. Dahiya, Does nuclear medium affect the transverse momentum-dependent parton distributions of valence quark of pions?, *Phys. Lett. B* **859**, 139114 (2024), arXiv:2409.05394 [hep-ph].

[54] S. Puhan, N. Kaur, A. Kumar, S. Dutt, and H. Dahiya, Pion valence quark distributions in asymmetric nuclear matter at finite temperature, *Phys. Rev. D* **110**, 054042 (2024), arXiv:2408.07334 [nucl-th].

[55] J. P. B. C. de Melo, K. Tsushima, B. El-Bennich, E. Rojas, and T. Frederico, Pion structure in the nuclear medium, *Phys. Rev. C* **90**, 035201 (2014), arXiv:1404.5873 [hep-ph].

[56] J. P. B. C. de Melo, K. Tsushima, and I. Ahmed, In-Medium Pion Valence Distributions in a Light-Front Model, *Phys. Lett. B* **766**, 125 (2017), arXiv:1608.03858 [hep-ph].

[57] P. T. P. Hutaizuk, J. J. Cobos-Martínez, Y. Oh, and K. Tsushima, Valence-quark distributions of pions and kaons in a nuclear medium, *Phys. Rev. D* **100**, 094011 (2019), arXiv:1908.02406 [hep-ph].

[58] P. T. P. Hutaizuk and S.-i. Nam, Gluon and valence quark distributions for the pion and kaon in nuclear matter, *Phys. Rev. D* **105**, 034021 (2022), arXiv:2112.05435 [hep-ph].



[hep-lat].

[93] P. C. Barry, N. Sato, W. Melnitchouk, and C.-R. Ji, First Monte Carlo Global QCD Analysis of Pion Parton Distributions, *Phys. Rev. Lett.* **121**, 152001 (2018), arXiv:1804.01965 [hep-ph].

[94] I. Novikov *et al.*, Parton Distribution Functions of the Charged Pion Within The xFitter Framework, *Phys. Rev. D* **102**, 014040 (2020), arXiv:2002.02902 [hep-ph].

[95] A. Abdel-Rehim *et al.*, Nucleon and pion structure with lattice QCD simulations at physical value of the pion mass, *Phys. Rev. D* **92**, 114513 (2015), [Erratum: *Phys. Rev. D* 93, 039904 (2016)], arXiv:1507.04936 [hep-lat].

[96] C. Best, M. Gockeler, R. Horsley, E.-M. Ilgenfritz, H. Perlt, P. E. L. Rakow, A. Schafer, G. Schierholz, A. Schiller, and S. Schramm, Pion and rho structure functions from lattice QCD, *Phys. Rev. D* **56**, 2743 (1997), arXiv:hep-lat/9703014.

[97] W. Detmold, W. Melnitchouk, and A. W. Thomas, Parton distribution functions in the pion from lattice QCD, *Phys. Rev. D* **68**, 034025 (2003), arXiv:hep-lat/0303015.

[98] G. Martinelli and C. T. Sachrajda, A Lattice Calculation of the Pion's Form-Factor and Structure Function, *Nucl. Phys. B* **306**, 865 (1988).

[99] P. J. Sutton, A. D. Martin, R. G. Roberts, and W. J. Stirling, Parton distributions for the pion extracted from Drell-Yan and prompt photon experiments, *Phys. Rev. D* **45**, 2349 (1992).

[100] C. Han, H. Xing, X. Wang, Q. Fu, R. Wang, and X. Chen, Pion Valence Quark Distributions from Maximum Entropy Method, *Phys. Lett. B* **800**, 135066 (2020), arXiv:1809.01549 [hep-ph].

[101] M. Gluck, E. Reya, and I. Schienbein, Pionic parton distributions revisited, *Eur. Phys. J. C* **10**, 313 (1999), arXiv:hep-ph/9903288.

[102] M. Ding, K. Raya, D. Binosi, L. Chang, C. D. Roberts, and S. M. Schmidt, Symmetry, symmetry breaking, and pion parton distributions, *Phys. Rev. D* **101**, 054014 (2020), arXiv:1905.05208 [nucl-th].

[103] S.-i. Nam, Parton-distribution functions for the pion and kaon in the gauge-invariant nonlocal chiral-quark model, *Phys. Rev. D* **86**, 074005 (2012), arXiv:1205.4156 [hep-ph].

[104] A. Watanabe, T. Sawada, and C. W. Kao, Kaon quark distribution functions in the chiral constituent quark model, *Phys. Rev. D* **97**, 074015 (2018), arXiv:1710.09529 [hep-ph].